# Heterologous reporter expression in the planarian *Schmidtea mediterranea* through somatic mRNA transfection

Richard Nelson Hall[1,12], Uri Weill[2,12], Margarita Khariton[1], Sergio Leal-Ortiz[3], Leonard Drees[2], Chew Chai[1], Yuan Xue[1], Benyamin Rosental[4], Stephen R. Quake[1,5,6], Alejandro Sánchez Alvarado[7,8], Nicholas A. Melosh[3], Andrew Fire[9,10], Jochen C. Rink[2,*], Bo Wang[1,11,*]

[1]Department of Bioengineering, Stanford University, Stanford, CA, USA
[2]Department of Tissue Dynamics and Regeneration, Max Planck Institute for Biophysical Chemistry, Göttingen, Germany
[3]Department of Materials Science and Engineering, Stanford University, Stanford, CA, USA
[4]The Shraga Segal Department of Microbiology, Immunology, and Genetics, Faculty of Health Sciences, Center for Regenerative Medicine and Stem Cells, Ben Gurion University of the Negev, Beer-Sheva, Israel
[5]Department of Applied Physics, Stanford University, Stanford, CA, USA.
[6]Chan Zuckerberg Biohub, San Francisco, CA, USA.
[7]Stowers Institute for Medical Research, Kansas City, MO, USA
[8]Howard Hughes Medical Institute, Kansas City, MO, USA.
[9]Department of Pathology, [10]Department of Genetics, [11]Department of Developmental Biology, Stanford University School of Medicine, Stanford, CA, USA

[12]These authors contributed equally to this work.

*Correspondence should be addressed to J.C.R. (jochen.rink@mpibpc.mpg.de) and B.W. (wangbo@stanford.edu)

**Abstract**

Planarians have long been studied for their regenerative abilities, but they possess limited genetic tools due to challenges in gene delivery, expression, and detection, despite decades of work. We developed a toolbox for heterologous protein expression in planarian cells and in live animals. Specifically, we identified and optimized nanotechnological and chemical transfection methods to efficiently deliver mRNA encoding nanoluciferase into somatic cells, including planarian adult stem cells (neoblasts). The use of a luminescent reporter allowed us to quantitatively measure protein expression through spectroscopy and microscopy, thus overcoming the strong autofluorescent background of planarian tissues. Using this platform, we investigated the use of endogenous untranslated region (UTR) sequences and codon usage bias to post-transcriptionally alter gene expression. Our work provides a strong foundation for advancing exogenous gene expression and for the rapid prototyping of genetic constructs to accelerate the development of transgenic techniques in planarians.

## Introduction

Planarian flatworms have fascinated generations of scientists with their astounding regenerative abilities and have played a critical role in our efforts to understand stem cells and regeneration (Newmark & Sánchez Alvarado, 2002; Reddien, 2018; Rink, 2018). Planarians can regenerate their entire body from a small tissue fragment. During this process, they restore their body axes and rebuild organs with appropriate proportions using a population of adult pluripotent somatic stem cells called neoblasts (Baguñà et al., 1989; Wagner et al., 2011; Zeng et al., 2018). In sexual strains, neoblasts also regenerate germ cells, breaching the Weissman barrier that separates soma and germline (Wang et al., 2007). While gene knockdown by RNA mediated genetic interference (RNAi) and sequencing techniques have been widely used in planarian research (Sánchez Alvarado & Newmark, 1999; Reddien et al., 2005; Collins et al., 2010; Böser et al., 2013; Duncan et al., 2015; Lakshmanan et al., 2016; Molinaro & Pearson, 2016; Grohme et al., 2018; Fincher et al., 2018; Plass et al., 2018; Mihaylova et al., 2018; Pascual-Carreras et al., 2020), tools for transgene expression have yet to be developed. Earlier efforts have used electroporation in whole animals (González-Estévez et al., 2003), and more recently in purified neoblasts under improved culture conditions (Lei et al., 2019). However, the lack of orthogonal verification of transgene expression combined with the intense autofluorescence of planarian tissue has limited the practical utility of both studies. It is unclear whether the issue is technical, owing to the vast range of experimental conditions to be explored, or biological, as a result of efficient gene silencing in planarians (Kim et al., 2019). Therefore, establishing a robust and quantitative positive control of transgene expression is still a paramount challenge in the planarian field.

Although transgene expression has become commonplace in many model organisms, establishing transgenesis *de novo* requires solving three coupled challenges: gene delivery, expression, and detection. Construct delivery and expression are necessary prerequisites for transgene detection. Conversely, developing delivery and expression methods are impossible without sensitive and quantitative detection methods (e.g., evaluating promoter activity requires a validated transgenic reporter, but measuring reporter expression requires a well characterized promoter). Therefore, the initial demonstration of transgene expression is essential as it can

transform the task of method development from a blind pursuit into a well constrained problem of parameter optimization.

For delivery, most transgenesis protocols begin by injecting a zygote; however, this is challenging in sexual planarians given that their zygotes are dispersed among numerous yolk cells (Cardona et al., 2006; Davies et al., 2017). Furthermore, the commonly used planarian strains are exclusively asexual, reproducing through fission and regeneration (Vila-Farré & Rink, 2018; Arnold, Benham-Pyle et al., 2019), making somatic cell transfection the only option. Such transfection methods, however, are primarily optimized for vertebrate tissues and immortalized cell lines. Here, to address the problem of delivery, we used a direct nanoscale injection method to first establish a reference in delivering nucleic acids into planarian cells. Based on this reference, we tested many other methods and identified several chemical transfection reagents that also showed high delivery efficacy.

A parallel challenge is that measuring functional gene delivery often relies on expression as the ultimate readout for efficiency. Due to the distant relationship between planarians and other model organisms, it is unclear whether utilizing ubiquitously expressed reporter constructs used in other research organisms would be sufficient. Furthermore, transgenes can be epigenetically modified and silenced through endogenous mechanisms, as has been noted in other systems like mouse and *C. elegans* (Chen et al., 2003; Aljohani et al., 2020). Therefore, we chose to transfect *in vitro* synthesized mRNA to circumvent the numerous variables associated with DNA based methods, such as nuclear import, transcription, and splicing, as well as for rapid expression due to the limitations of planarian cell culture (Lei et al., 2019).

Finally, planarian autofluorescence limits the utility of commonly used fluorescent reporters, especially during the initial stages of reporter optimization when signals may be weak. To overcome this detection challenge, we used an alternative strategy which relies on luminescence. Nanoluciferase (Nluc), derived from the deep sea shrimp *Oplophorus gracilirostris*, is a compact (19 kDa) and stable luciferase which is orders of magnitude brighter than other luciferases (England et al., 2016). This allows for high signal-to-noise quantification of luminescence from Nluc expression, so even weak signals can be detected to guide further optimization.

Combining all these technical advances, we have established a robust means for exogenous expression in both cell cultures and live animals of the planarian model species *Schmidtea mediterranea*. Taking advantage of the sensitivity of our Nluc expression assay, we quantified the influence of adding endogenous planarian untranslated regions (UTRs) and changed codon usage bias to manipulate and optimize transgene expression through a wide dynamic range. Our results not only provide the first positive control for exogenous gene expression in planarians to guide the future development of planarian transgenesis, but also offer a new route to manipulate the functional transcriptome in planarian cells. We anticipate that our strategies may also prove useful in other asexually reproducing animals which lack a germline and cannot otherwise be transformed through embryonic manipulations.

## Results

### *Nanoluciferase mRNA delivered through nanostraws is expressed in planarian cells*

In order to establish mRNA expression in the asexual strain of *S. mediterranea*, we sought to identify an efficient and species-agnostic platform for delivering genetic material into primary planarian cells. We selected nanostraws, which combine the robustness of mechanical methods like microinjection with the throughput of electrical methods like electroporation (Tay & Melosh, 2019).

Nanostraws are approximately100-200 nm wide hollow aluminum oxide tubes protruding from a polycarbonate substrate situated above a buffer reservoir containing the genetic material to be delivered (**Figure 1A-B**). Cells are centrifuged against the straws which engage in close contact with the cell membrane. Electric pulses are then used to locally porate the membranes and electrophorese genetic material through the nanostraws and directly into the cellular cytoplasm (**Figure 1 – figure supplement 1**). By only permeabilizing membranes immediately in contact with nanostraws, they have been shown to improve both delivery efficiency and viability of transformed cells (Xie et al., 2013; Cao et al., 2018).

To prepare cells for nanostraw delivery, we flow-sorted a neoblast enriched population (so-called X1FS) from dissociated planarians (Wagner et al., 2011). The resulting cells were uniform in size and depleted of debris, which are important preconditions for nanostraw delivery. Our initial experiments used capped and polyadenylated *in vitro* transcribed mRNA encoding the red fluorescent protein, mScarlet, fused to the planarian histone H2B (**Supplementary Table 1**). We reasoned that red fluorescence might be more easily detectable against planarian autofluorescence, which is biased towards shorter wavelengths, and that a nuclear localization signal might further enhance signal to noise. Initial experiments used a pulse train protocol that was empirically optimized for delivery in human hematopoietic stem cells, which have similar morphological characteristics to neoblasts (i.e., small size, minimally adherent, high nucleus to cytoplasm ratio) (Schmiderer et al., 2020).

Microscopic examination of the transfected cells showed a weak and sometimes nuclear localized fluorescence. However, negative controls also contained similarly fluorescent cells

(**Figure 1C**). Therefore, we performed flow cytometry analysis to quantify fluorescence signal and found, even in this relatively uniform cell population, a broad distribution of fluorescence intensity, spanning three orders of magnitude in both experimental and negative conditions (**Figure 1D**). This highly variable autofluorescence in our measurements highlights the difficulties of using fluorescent reporters. Since some cells genuinely exhibit brighter fluorescence than others, false positives may be common and true positives could be obscured by the broad autofluorescent background such that H2B-mScarlet expression cannot be unambiguously assessed. Together, these results compelled us to seek an alternative non-fluorescent reporter to quantify gene expression in planarian cells.

Unlike fluorophores, luciferases produce light as the result of an oxidative chemical reaction with an exogenously added substrate (luciferin), and most animal tissues are devoid of auto-luminescence due to the enzymatic nature of luciferases (**Figure 1E**). To take advantage of the high signal-to-noise ratios achievable with luminescence-based reporters, we delivered capped and polyadenylated mRNA encoding a planarian codon optimized nanoluciferase (sNluc1) (**Supplementary Table 1**) into X1FS cells and transfected them as was done previously with H2B-mScarlet mRNA. Transfected cells were maintained for 24 hrs in Iso-L15, a nutrient rich medium with reduced osmolarity. A similar medium has been shown previously to improve planarian cell viability and maintain neoblast pluripotency (Lei et al., 2019). Strikingly, we saw that transfected cells produced a clear and reproducible luminescence signal over 100-fold above the background signal of the negative controls. Moreover, the physical dimensions of the nanostraws strongly influenced the signal intensity, as has been observed in previous nanostraw transfection experiments (Xie et al., 2013), implicating that we were in the regime where expression was dependent on the amount of mRNA delivered (**Figure 1F**). Overall, our results provide unambiguous proof-of-principle for heterologous protein expression in planarian cells.

***A screen identifies chemical reagents to efficiently transfect planarian cells***

With a validated reporter construct in hand, we next sought to identify a more broadly accessible mRNA delivery method. Chemical transfection reagents have become increasingly popular because of their ease of use, high efficiency, and scalability, but they are often developed and optimized for specific cell types.

To identify suitable reagents for planarian cell transfection, we screened a panel of commercially available reagents by transfecting *in vitro* transcribed sNluc1 mRNA containing 5' and 3' UTR sequences from the highly expressed planarian gene, YB1 (**Supplementary Table 1**). Our screen used total cells from freshly dissociated animals rather than X1FS cells due to the large number of individual transfections needed. Initially, all reagents were utilized according to the manufacturer's recommended protocols (**Supplemental Table 2**). While most transfections had little to no effect, Viromer and Trans-IT (Mirus) reagents consistently achieved luminescent signals 100 to 1,000-fold above the negative control (**Figure 2A**).

To confirm that luminescent signals in the chemical transfections indeed measured Nluc expression in planarian cells, we exposed Trans-IT transfected total cells 24 hr post transfection (hpt) to NanoGlo-Live furimazine substrate (Promega) and imaged the cultures on an LV200 bioluminescence imaging system (Olympus). Individual luminescent cells positive for the live cell indicator Calcein AM were apparent in Trans-IT transfections but never observed in controls (**Figure 2B**). High magnification luminescence imaging confirmed the cytoplasmic origin of the luminescence signal. These observations establish chemical delivery as a viable method for mRNA transfection of planarian cells, with Viromer and Trans-IT as promising leads.

To further optimize Nluc expression, we tested various ratios between Nluc mRNA and reagent components (**Figure 2C-D**). For Viromer, increasing both the amount of reagent and/or mRNA in the transfection mix doubled the baseline signal, with 0.8 µL reagent per 1 µg mRNA per reaction as an economic compromise for further experiments. A similar two-fold boost over the baseline signal was also achieved for Trans-IT, but maximal signal intensities in cell cultures remained below those achieved by Viromer transfections. To investigate the kinetics of exogenous mRNA expression in both regimens, we performed time course experiments. Luminescence was apparent as early as 4 hpt for both reagents, consistent with the expected kinetics of mRNA transfection and translation. Luminescence continued to increase past the last assayed time point at 72 hpt, which was surprising given the short transcript half-life, suggesting that transfected Nluc mRNA is stable in the transfection complex and/or inside planarian cells, allowing for sustained transfection and expression (**Figure 2E-F**).

Finally, with the planarian's prominence as a model for studies of regeneration, we sought to determine whether neoblasts were amenable to chemical transfection. In the absence of detectable anti-Nluc immunostaining or live imaging compatible with neoblast markers, we compared the luminescence signal produced between parallel Viromer transfections of neoblast enriched (X1FS) cell populations and an equal number of total cells. Both conditions showed comparable signal 24 hpt. Since X1FS is not a pure population of neoblasts, and luminescence may be coming from differentiated cells in the sample, we developed a new sorting strategy to isolate a cell population (CRNeoblasts) containing approximately 94% *piwi-1*$^{+}$ cells (**Figure 2 – figure supplement 1**). When transfected and assayed 24 hpt, CRNeoblasts showed approximately 25% of the expression measured in the bulk population, suggesting that neoblasts can be transfected by our method. Altogether, these results establish chemical transfection to deliver mRNA into planarian cells including neoblasts, the ease and scalability of which provide a strong basis for further optimization of planarian transgene expression.

***Untranslated regions and codon optimization can modulate expression of delivered mRNA***

We next examined the influence of post-transcriptional regulators of gene expression such as UTRs and codon usage bias, which can be exploited to further increase Nluc expression. The ability to transfect and express exogenous mRNA also opens new possibilities for the analysis of gene regulation in planarians, which have so far been limited to observing phenotypic changes and measuring net RNA depletion under the influence of RNAi.

First, we considered non-coding regions, such as the 5' and 3' UTRs, which can restrict gene expression to specific cell types (Brun et al., 2003; Merritt et al., 2008) and can contain targets of small RNA silencing pathways (Diag et al., 2018). To identify UTR elements that can significantly alter Nluc expression, we utilized expression data and genomic mappings available on PlanMine (Rozanski et al., 2019) to identify four endogenous genes with high expression across both neoblasts and differentiated cell types, reasoning that they may enhance Nluc mRNA stability and/or translation efficiency in total cell transfections. We also limited our search to shorter genes which mapped uniquely to the genome, allowing them to be more easily isolated via PCR. We cloned the 5' and 3' UTRs to flank sNluc1 (**Figure 3 – figure supplement 1**) and

produced capped and polyadenylated mRNA from these templates (**Figure 3 – figure supplement 2**). We found that UTRs either increased (RPL15, YB1, RPL10) or decreased (ENO) expression of Nluc relative to the construct lacking endogenous UTRs (No UTR condition, see **Supplementary Table 3** for sequence details) demonstrating the significant influence of UTRs on planarian transgene expression (**Figure 3A**). Further, the 3-fold signal boost granted by RPL15 UTRs suggests that these sequences are promising starting points for further expression optimization.

Second, we considered codon optimization, the commonplace practice of altering synonymous codons of a transgene to better match the preferences of the host organism in order to increase expression. Codon composition has been shown to modulate translation kinetics and mRNA stability (Quax et al., 2015; Jeacock et al., 2018); moreover, the global A/T-bias in the genome (70% A/T) and a strong preference for A/T at wobble positions make codon optimization an important consideration in *S. mediterranea*. To investigate this effect, we generated another five codon optimized variants in addition to the baseline Nluc construct that cover a range of codon adaptation indices (CAI), a 0-1 bounded value measuring the genes codon bias compared to a reference codon preference table (Puigbò et al., 2008) (**Supplementary Table 1**). We also included a Nluc sequence optimized for mammalian expression as a reference for comparison. Genes with higher CAI values tended to have lower GC content, reflecting the A/T bias in *S. mediterranea* genome (**Supplementary Table 1**) (Grohme et al., 2018).

The luminescence quantifications in total live cell transfections did not reveal the expected correlation between luminescence signal and CAI (Jeacock et al., 2018). Instead, the construct with the highest CAI (sNluc0; 0.905) showed the weakest expression, while hNluc, optimized for expression in human cells, with an accordingly poor planarian CAI of 0.509, was the second most highly expressed (**Figure 3B**). The most highly expressed construct (sNluc2; CAI = 0.725) was part of a series of constructs, with very similar CAIs and GC content, generated by randomly sampling the planarian codon table (sNluc2-4; **Supplementary Tables 1, 3**). These results hint at a complex relationship between codon usage bias and gene expression in planarians; nevertheless, they provide us with a coding sequence (sNluc2) that provides about approximately 2 fold higher expression than the original baseline (sNluc1) construct.

After observing variations between constructs with different UTRs and codon optimized Nluc sequences, we asked whether their effects might be additive. To this end, we constructed a range of combined constructs mixing UTRs and codon optimized Nluc sequences and assayed their expression in total cells (**Figure 3C**). Although the "best of both" construct (RPL15-sNluc2) had the highest average expression, it did not show a significant difference compared to other constructs. Moreover, the stark difference between the UTR effects of ENO (worst) and RPL15 (best) disappeared when combined with sNluc2. The "worst" codon-optimized sNluc0 in combination with RPL15 UTRs was also expressed at a level comparable to the other constructs. Overall, these results highlight the complex interactions between different construct design variables. Regardless, they identify RPL15-sNluc2 as an improved reporter construct for future experiments.

By testing the effects of UTR sequences, codon optimization, and combinations thereof, we have demonstrated a framework for investigating post-transcriptional factors modulating the expression of exogenously introduced mRNAs in planarians. Furthermore, we anticipate that the optimizations made here will hold true for DNA-based transgenic methods in the future.

***Heterologous reporter expression in vivo***

Although the ability to transfect planarian cells with mRNA *in vitro* represents a significant advance in the genetic manipulation of planarian cells, the lack of neoblast proliferation in culture limits the range of questions that can be addressed *in vitro*. We therefore explored whether our transfection protocols might be sufficient for generating detectable reporter expression *in vivo*.

We injected RPL15-sNluc2 mRNA complexed with Viromer or Trans-IT into the parenchymal tissue along the tail midline, which reduces the risk of misinjections into the abundant gut branches. We then measured luminescence on individually dissociated worms at multiple time points post-transfection (**Figure 4A**). The luminescence background in tissue lysates from sham-injected animals was universally very low, mirroring what was observed *in vitro*. In contrast, mRNA injection with Viromer or Trans-IT led to luminescence signals up to 100-fold above

background (**Figure 4B**). For Viromer, the highest fraction of expressing animals was detected already at 12 hpt (13/30 hpt) and tapered to 4/30 after 72 hpt (**Figure 4B**). Contrary to our observations *in vitro*, Trans-IT transfections produced luminescence comparable to Viromer, with similar kinetics and fraction of expressing animals (**Figure 4C**), suggesting that for *in vivo* transfections, Trans-IT can be as effective as Viromer. The early peak and rapid decline in luminescence intensity represents another difference compared to our previous *in vitro* experiments and may be due to the reduced stability of transfection complexes *in vivo* or efficient clearing of the transfection complexes by the planarian excretory system (Thi-Kim Vu et al., 2015).

We next asked whether Nluc expression in live worms was sufficient for luminescence imaging. Initial experiments showed that customary concentrations of the cell-permeable substrate furimazine are well-tolerated by planarians, with no overt signs of toxicity even after overnight incubations, which makes live imaging feasible. Injected worms were anaesthetized with linalool, incubated for 15 min in furimazine solution, agarose-mounted on glass bottom dishes, and imaged on a luminescence microscope. This experiment revealed bright luminescence in both Viromer and Trans-IT-injected animals, while no luminescence was detected in negative controls injected with mRNA alone (**Figure 4D**). The success rate observed through imaging (~30%) matched our results from the plate reader assay. Moreover, luminescence was always found within the vicinity of the tail injection site as expected if the signal were from Nluc mRNA uptake and expression. Although the spatial resolution of *in vivo* luminescence imaging did not allow for cellular resolution, the size of the injected region in the maximum projections was ~50 µm and consistent with the transfection of a small cluster of cells immediately adjacent to the injection site. All together, these experiments demonstrate proof-of-principle for mRNA reporter delivery and expression in live planarians.

## Discussion

Transgene expression in planarian flatworms has been a persistent challenge in the field since the molecular biology revival of the system around two decades ago (Agata & Watanabe, 1999; Newmark & Sánchez Alvarado, 2002). Here, we accomplished proof-of-principle heterologous protein expression in the planarian model species *S. mediterranea* by combining three

experimental approaches: (1) nanostraw electro-delivery to establish an initial positive control, which enabled subsequent optimization of chemical delivery methods; (2) delivering mRNA instead of DNA to bypass the complexities of nuclear import, transcription, and splicing, and optimizing post-transcriptional processes for enhanced expression; and (3) using a luminescent reporter to circumvent the strong autofluorescence which complicates the use of fluorescent reporters. By making these choices, we observed a clear signal from an exogenously supplied Nluc mRNA in both planarian cells *in vitro* and *in vivo*.

Exogenous reporter expression in our results is supported by multiple independent lines of evidence. First, we showed that planarians are minimally autoluminescent, and most experimental conditions tested reproducibly reached luminescence intensities as high as 3-4 orders of magnitude above the background. Second, we observed that the luminescence showed a dose-dependence on Nluc mRNA amounts and exhibited rapid expression kinetics characteristic of mRNA expression. Third, luminescence intensity was modulated by biologically relevant factors such as UTR sequences and codon usage. Fourth, imaging of transfected cell cultures confirmed a cytoplasmic origin of the luminescence signal. Fifth, we succeeded in imaging luminescence in injected live worms, with the signal consistently restricted to the injection site. Finally, the results presented in this manuscript were gathered in two different laboratories, which highlights the robustness and general applicability of the technique. Collectively, our results represent the first robust demonstration of exogenous mRNA expression in planarians.

In terms of applications, our current reporter assay already represents a significant expansion of the planarian toolkit. Besides UTRs, our protocol allows for exploring other post-transcriptional gene regulatory mechanisms in planarians. For example, incorporating trans-spliced 5' leader sequences (Zayas et al., 2005; Rossi et al., 2014), adding target sites of known small RNAs (Kim et al., 2019), including internal ribosomal entry sites (IRES), or manipulating secondary structures of mRNA (Leppek et al., 2021) may enable the identification of modulatory elements that have a stimulatory or suppressive effect on mRNA function and expression. Indeed, our observation that CAI and expression were not well correlated, along with the non-additive effects of UTRs and codon usage (**Figure 3B-C**), suggests that a complex set of sequence factors

influence the expression of exogenous mRNA. Our platform allows for the systematic characterization and analysis of these factors to better predict how sequence informs expression. Another important direction is to investigate the effect of modified nucleotides, which is gaining traction as a means of increasing RNA expression and stability (Andries et al., 2015; Svitkin et al., 2017). In fact, we have already compared transfections with RPL15-sNluc2 mRNA incorporating the canonical uridine versus mRNA with the base analog 1-methyl pseudouridine (m1Ψ). While we did not observe any significant changes in gene expression (**Figure 3 – figure supplement 3**), our protocol provides a route to explore the effects of other modified nucleotides on mRNA expression in planarian cells. Finally, while overexpression is desirable for labeling and imaging purposes, many endogenous genes are expressed at much lower levels than most constitutively active transgenic constructs might drive. In this sense, it will be important to explore whether current expression levels are sufficient for achieving neomorphic phenotypes, such as ectopic expression of Wnt or other signaling proteins with essential roles in planarian body patterning (Petersen & Reddien, 2009; Stückemann et al., 2017).

A direct utility of our method is to provide a robust positive control and a baseline for further optimization of gene delivery and reporter expression in planarians. First, utilizing RNA-based synthetic biology tools like self-replicating RNA replicons including alphavirus (Beal et al., 2015; Li et al., 2019) and nodavirus (Taning et al., 2018) may significantly enhance mRNA driven expression, which is currently still transient and limited to small fractions of cells, as observed in our *in vitro* imaging and *in vivo* transfection experiments (**Figure 2C**). Such tools may enable increased expression to levels detectable through western blot or fluorescence reporters. Second, specialized delivery protocol and expression constructs might be required to optimize expression in specific cell types. Our study provides a simple procedure to quickly isolate a highly pure population of neoblasts (**Figure 2 – figure supplement 1**) which opens the possibility for identifying and optimizing transfection protocols specifically tailored for targeting neoblasts. Third, with luminescence as a readout, DNA based transgene expression can be quantitatively evaluated against an mRNA-based control. Constructs developed in this work can also serve as the foundation for the design of DNA encoded reporters. Fourth, the ability to deliver and express mRNA *in vivo* also opens the door to testing various genome editing strategies such as CRISPR and transposon integration by co-transfecting Cas9 mRNA with a

repair template or transposase mRNA with an integration cassette, respectively. Finally, we anticipate that further screens of transfection reagents using our constructs will allow for the identification of other, potentially more effective, alternatives, and remove our current dependence on a limited set of reagents. We note that Viromer reagents are no longer commercially available since the supplier's (Lipocalyx) acquisition by BioNTech, one of the SARS-CoV-2 mRNA vaccine producers. Although Viromer reagents are still available through our labs upon request and Trans-IT (Mirus) reagent is equally effective at least for *in vivo* transfection, there is an obvious need to enrich our options.

Altogether, our method proves conclusively that transgene expression is possible in the planarian model species *S. mediterranea*. Our study provides a validated reporter construct, a quantitative expression assay, and several transfection reagents, which collectively narrow the enormous parameter space that make the *de novo* establishment of transgenesis in phylogenetically distant model systems so challenging. As such, our results transform the quest for planarian transgenesis from a blind trial-and-error process into a constrained parameter optimization process, which we hope to proceed rapidly within our community.

## Materials and Methods

**Planarian cell dissociation.** Planarian cells were prepared by finely mincing the worm with a razor blade and suspending the tissue in CMF (Ca/Mg-Free media: $NaH_2PO_4$ 480 mg/L, NaCl 960 mg/L, KCl 1.44 g/L, $NaHCO_3$ 960 mg/L, HEPES 3.57 g/L, D-glucose 0.24 g/L, BSA 1 g/L, pH 7.4 in MilliQ $H_2O$). The tissue was rocked for 5 min, followed by gentle pipetting for 10 min, or until the tissue was visibly homogenized. The cells were centrifuged at 250 g for 4 min, and the supernatant was removed and replaced with 1.5 mL of fresh CMF. The cell suspension was then serially filtered through 100, 70, 40, and 30-µm mesh strainers. The filtered cell suspension was centrifuged and transferred to Iso-L15 (1:1 Leibovitz's L-15 to MilliQ $H_2O$, 1× MEM nonessential amino acids, 1× antibiotic-antimycotic, 1× MEM vitamin solution, 1 mM Sodium Pyruvate, 2.5 g/L HEPES, 5% FBS, buffer to pH 7.8).

**FACS.** To isolate neoblast-enriched X1FS population, an aliquot of sacrificial cells was stained with Hoechst 33342 (10 µg/mL) in CMF for 15 min, filtered, and sorted on a Sony SH800 with either the 100 or 130 µm sorting chip (LE-C3210, LE-C3213, Sony). Following the identification of the neoblast population using Hoechst fluorescence (Wagner et al., 2011), unstained planarian cells were loaded and sorted using the neoblast gate overlayed on the forward and side-scatter into Iso-L15 medium. After sorting, the cells were centrifuged at 250 g for 5 min and resuspended in fresh Iso-L15.

To isolate CRNeoblasts, dissociated planarian cells at a density of $1\text{-}5\times10^6$ cells/mL were stained with 1:500 (5 µM) CellRox Green (Invitrogen, C10444) and 1:7000 (143 nM) LysoTracker Deep Red (Invitrogen, L12492). The sample was rocked gently in the dark for 30 min at room temperature. After incubation, the cells were pipetted up and down before being strained through a 30 µm filter cap FACS tube. The cells were sorted on a Sony SH800 with a 100 µm sorting chip. Cells were first gated by forward and side-scatter, then a final gate around CellRox Green high and LysoTracker Deep Red low identified the CRNeoblast population (**Figure 2 – figure supplement 1**).

**Single-cell RNA-seq analysis of CRNeoblast.** Single cell SmartSeq2 protocol was carried out as previously described (Li et al., 2021). Paired-end reads were mapped to dd_Smed_v6 reference transcriptome (Rozanski et al., 2019) using Salmon (v1.4.0) (Patro et al., 2017). Downstream preprocessing and analysis were performed using estimated counts in the Salmon output, for which we sum up counts from different isoforms of the same gene. Cells with fewer than 2,400 genes detected were filtered out, passing 481 cells for downstream analysis. Raw gene counts were then normalized for sequencing coverage such that each cell has a total read count equal to that of the median library size for all cells. The resulting counts were added with a pseudo count of 1 and log-2 transformed. 2D embedding was performed with the SAM algorithm (version 0.8.1) (Tarashansky et al., 2019) using default parameters. *piwi-1*$^{+}$ cells were defined as those for which their log-2 transformed and normalized read counts were greater than zero. *piwi-1*$^{+}$ cells were clustered using the Leiden clustering algorithm, and each cluster was annotated using progenitor marker genes previously identified (N_epidermal: *soxP3*, dd_Smed_v6_5942_0_1; N_gut: *hnf*, dd_Smed_v6_1694_0_1; N_muscle: *pcdh11*, dd_Smed_v6_9283_0_1, cNeoblast: *tgs1*, dd_Smed_v6_10988_0_1).

**Nanostraw electro-delivery.** Nanostraws were fabricated according to previously established methods (Cao et al., 2018). Each nanostraw cartridge was loaded with 200,000 X1FS cells in 300 µL of Iso-L15 media and centrifuged at 300 g for 10 min to ensure close contact between straws and cells. For each cartridge, 3 µg of *in vitro* synthesized mRNA was diluted in PBS to a total volume of 35 µL and placed on the titanium anode, and a cartridge was carefully lowered onto the mRNA solution. The titanium cathode was placed atop, and the electro-delivery assembly was subjected to a 35 V, 200 µs, 40 Hz square wave pulse 3 times for 45 s each, with a 1 min rest in between pulses. Transfected cells were incubated at 20°C in the dark for 24 hr before being transferred from the nanostraw cartridge to a 96 well plate for assaying luminescence.

**Chemical transfection.** For *in vitro* experiments, dissociated planarian cells were suspended at a concentration of $0.88\times10^{6}$ cells/mL in Iso-L15 medium supplemented with 10 µg/mL ciprofloxacin. 225 µL of cell suspension was added to each well of a 96 well plate for a total of approximately 200,000 cells per well. For the initial screen, each reagent was prepared as specified in **Supplementary Table 2**. After adding transfection complexes to each well, the cells

were incubated at 20°C in the dark before assaying luminescence. For live animal injections, transfection mixture was loaded on needles pulled from glass capillaries (Drummond). Needles were loaded on a FemtoJet injection system (Eppendorf) and worms were injected with 900 nL transfection mix. Worms were left to rest in the dark at 20°C until assaying.

**Nanoluciferase assay.** For dissociated cells, luminescence was measured using the NanoGlo Live Cell Assay (Promega). Furimazine substrate was added to NanoGlo buffer at a ratio of 1:20, and 25 µL of reagent was added to 250 µL of transfected cells. For live planarians, each injected worm was individually dissociated by finely mincing the worm with a razor blade and suspending the tissue in 250 µL Iso-L15 medium just prior to assaying. The resuspended tissue was transferred to a 96-well white bottom plate. Nluc expression was measured using the NanoGlo Assay Lysis (Promega) kit. Furimazine substrate was added to the NanoGlo lysis buffer at a ratio of 1:50 and 100 µL of reagent was added to the cells. Cells were lysed by pipetting up and down 10 times. Luminescence was measured on a plate reader (BioTek HTX, or BioTek Synergy™ Neo2, or EnVision Microplate Reader). Integration time was set at 1 s and the digital gain was kept consistent on each instrument for all experiments.

**Luminescence imaging.** For imaging planarian cells *in vitro,* Nluc expression was imaged using the NanoGlo Live Cell Assay. 35 mm glass-bottom dishes were coated with 0.5 mg/mL Concanavalin A (Sigma-Aldrich) dissolved in deionized water for 2 hrs, washed, and air dried. Transfected cells were transferred to the coated dish in a total of 1 mL of Iso-L15, allowed to adhere to the glass surface for 1 hr, and stained with Calcein AM (ThermoFisher) (4 ng/ µL) to label live cells. 12.5 µL of NanoGlo live (Promega) substrate was added to 237.5 µL of NanoGlo buffer, mixed, and then added to the media. Cells were imaged using an LV200 Bioluminescence Imaging System (Olympus) with a 20× air objective (Olympus: UPLXAPO20X) or a 100× oil immersion objective (Olympus: UPLXAPO100XO). For *in vivo* imaging, NanoGlo live (Promega) substrate was added to planarian water with 1% DMSO at a ratio of 1:20. Worms were incubated in 100 µL of reagent mixture for 15 min, and then mounted on glass bottom dishes, embedded in agarose gel (1.5%) supplemented with 1:5000 linalool and 1:20 furimazine substrate, which was covered with a cover slip. They were imaged for luminescence and brightfield using an LV200 with a 20× air objective (Olympus: UPLXAPO20X).

**Cloning.** To generate a plasmid capable of *in vitro* transcription and for harvesting the endogenous regulatory sequences (5' and 3' UTRs) of planarian genes, we first amplified the backbone of pDONOR221 (ThermoFisher) using primers BW-NH-104-105 (all primer sequences are provided in **Supplementary Table 4**), as well as the LacZ cassette from pUC19 (Addgene #50005) with a T7 promoter sequence followed by a BsaI restriction site for subsequent cloning steps, all flanked between BbsI restriction sites and M13 forward and M13 reverse primer sites (for *in vitro* transcription template production) using primers BW-NH-106-107. The amplified backbone was digested with BsaI-HF (NEB) and the LacZ insert was digested with BbsI-HF (NEB). The digested backbones were purified using the Zymo Clean and Concentrate kit (Zymo). The purified fragments were ligated together using T4 DNA Ligase (NEB) to create pNHT7 (**Figure 3 – figure supplement 1A**).

We cloned the gene of interest (GOI) from a pool of planarian cDNA using primers (BW-NH-108-125) containing BsaI restriction sites to produce overhangs compatible with pNHT7. The amplicons were purified using the Zymo Clean and Concentrate kit and then inserted into pNHT7 via a golden gate reaction containing 40 ng of backbone and 20 ng for each insert to be cloned in a 20 µL reaction volume containing 2 µL T4 Ligase Buffer, 1 µL T4 DNA Ligase, and 1 µL BsaI-HF to produce pNHT7::GOI (**Figure 3 – figure supplement 1B**).

Finally, to insert a reporter between the 5' and 3' UTRs, we amplified pNHT7::GOI with outward facing primers (BW-NH-128-139) which bind to the end and beginning of the 5' and 3' UTRs respectively containing the BsaI restriction sites. The reporter was then amplified to append compatible BsaI restriction sites using primers BW-NH-174-185 and inserted between the two UTR sequences via a golden gate reaction. The resulting plasmid was amplified with M13 forward and M13 reverse primers to produce linear template for *in vitro* transcription reactions (**Figure 3 – figure supplement 1C**).

***In vitro* transcription.** *In vitro* transcription was performed using the T7 mScript™ Standard mRNA Production System (CELLSCRIPT, C-MSC100625) according to the manufacturer's protocol, opting for a 1 hr incubation during T7 transcription, a 2 hr incubation for 5' capping,

and a 1 hr incubation for poly-A tailing. RNA purification was performed by adding 600 µL of ethanol to 50 µL of 10 M ammonium acetate. A standard 60 µL reaction typically yields 60 µg of mRNA. For expected results, see **Figure 3 – figure supplement 2**. For mRNA containing m1Ψ, the rNTP mix provided in the CELLSCRIPT kit was substituted for a homemade mixture of rNTPs containing 10 mM rGTP, 10 mM rCTP, 10 mM rATP, and 10 mM m1Ψ (TriLink).

**Acknowledgements**

We thank K. Lei, C. Kuhn, A. Voskoboynik for stimulating discussion, E. Liu and D. Burghardt for experimental assistance, Y. Lim and T. Boothe for microscopy assistance. RNH and CC are supported by NSF Graduate Research Fellowships. UW is supported by an EMBO Long-Term Fellowship. BW is Beckman Young Investigator. UW, LD, and JCR are supported by the Max Planck Society. AF is supported by a NIH grant (R35GM130366). BW and BR thank the support from a HFSP grant (RGY0085/2019). This work was initiated through a Stanford Bio-X Interdisciplinary Initiative seed grant (IIP9-64) to BW, AF, and NAM, and later supported by an NSF EDGE grant (IOS-1923534) to BW, ASA, and NAM, and a Volkswagen Foundation grant (Az.-99498) to JCR.

## References


Agata, K., & Watanabe, K. (1999). Molecular and cellular aspects of planarian regeneration. *Seminars in Cell and Developmental Biology*, *10*(4), 377–383. https://doi.org/10.1006/scdb.1999.0324

Aljohani, M. D., El Mouridi, S., Priyadarshini, M., Vargas-Velazquez, A. M., & Frøkjær-Jensen, C. (2020). Engineering rules that minimize germline silencing of transgenes in simple extrachromosomal arrays in *C. elegans*. *Nature Communications*, *11*, 6300. https://doi.org/10.1038/s41467-020-19898-0

Andries, O., Mc Cafferty, S., De Smedt, S. C., Weiss, R., Sanders, N. N., & Kitada, T. (2015). N1-methylpseudouridine-incorporated mRNA outperforms pseudouridine-incorporated mRNA by providing enhanced protein expression and reduced immunogenicity in mammalian cell lines and mice. *Journal of Controlled Release*, *217*(2015), 337–344. https://doi.org/10.1016/j.jconrel.2015.08.051

Arnold, C. P., Benham-Pyle, B. W., Lange, J. J., Wood, C. J., & Sánchez Alvarado, A. (2019). Wnt and TGFβ coordinate growth and patterning to regulate size-dependent behaviour. *Nature*, *572*(7771), 655–659. https://doi.org/10.1038/s41586-019-1478-7

Baguñà, J., Saló, E., & Auladell, C. (1989). Regeneration and pattern formation in planarians. III. that neoblasts are totipotent stem cells and the cells. *Development*, *107*(1), 77–86.

Beal, J., Wagner, T. E., Kitada, T., Azizgolshani, O., Parker, J. M., Densmore, D., & Weiss, R. (2015). Model-driven engineering of gene expression from RNA replicons. *ACS Synthetic Biology*, *4*(1), 48–56. https://doi.org/10.1021/sb500173f

Böser, A., Drexler, H. C. A., Reuter, H., Schmitz, H., Wu, G., Schöler, H. R., Gentile, L., & Bartscherer, K. (2013) SILAC proteomics of planarians identifies Ncoa5 as a conserved component of pluripotent stem cells. *Cell Reports*, *5*(4), 1142–1155. https://doi: 10.1016/j.celrep.2013.10.035

Brun, S., Faucon-Biguet, N., & Mallet, J. (2003). Optimization of transgene expression at the posttranscriptional level in neural cells: Implications for gene therapy. *Molecular Therapy*, *7*(6), 782–789. https://doi.org/10.1016/S1525-0016(03)00097-2

Cao, Y., Chen, H., Qiu, R., Hanna, M., Ma, E., Hjort, M., Zhang, A., Lewis, R. S., Wu, J. C., & Melosh, N. A. (2018). Universal intracellular biomolecule delivery with precise dosage control. *Science Advances*, *4*(10), eaat8131. https://doi.org/10.1126/sciadv.aat8131

Cardona, A., Hartenstein, V., & Romero, R. (2006). Early embryogenesis of planaria: A cryptic larva feeding on maternal resources. *Development Genes and Evolution*, *216*(11), 667–681. https://doi.org/10.1007/s00427-006-0094-3

Chen, Z. Y., He, C. Y., Ehrhardt, A., & Kay, M. A. (2003). Minicircle DNA vectors devoid of bacterial DNA result in persistent and high-level transgene expression in vivo. *Molecular Therapy*, *8*(3), 495–500. https://doi.org/10.1016/S1525-0016(03)00168-0

Collins III, J. J., Hou, X., Romanova, E. V., Lambrus, B. G., Miller, C. M., Saberi, A., Sweedler, J. V., & Newmark, P. A. (2010) Genome-wide analyses reveal a role for peptide hormones in planarian germline development. *PLoS Biology*, *8*(10), e1000509. https://doi: 10.1371/journal.pbio.1000509.

Davies, E. L., Lei, K., Seidel, C. W., Kroesen, A. E., McKinney, S. A., Guo, L., Robb, S. M. C., Ross, E. J., Gotting, K., & Sánchez Alvarado, A. (2017). Embryonic origin of adult stem cells required for tissue homeostasis and regeneration. *eLife*, *6*, e21052. https://doi.org/10.7554/eLife.21052

Diag, A., Schilling, M., Klironomos, F., Ayoub, S., & Rajewsky, N. (2018). Spatiotemporal m(i)RNA architecture and 3′ UTR regulation in the *C. elegans* germline. *Developmental Cell*, *47*(6), 785-800.e8. https://doi.org/10.1016/j.devcel.2018.10.005

Duncan, E. M., Chitsazan, A. D., Seidel, C. W., & Alvarado, A. S. (2015). Set1 and MLL1/2 target distinct sets of functionally different genomic loci in vivo. *Cell Reports*, *13*(12), 2741–2755. https://doi.org/10.1016/j.celrep.2015.11.059

England, C. G., Ehlerding, E. B., & Cai, W. (2016). NanoLuc: A small luciferase is brightening up the field of bioluminescence. *Bioconjugate Chemistry*, *27*(5), 1175–1187. https://doi.org/10.1021/acs.bioconjchem.6b00112

Fincher, C. T., Wurtzel, O., de Hoog, T., Kravarik, K. M., & Reddien, P. W. (2018). Cell type transcriptome atlas for the planarian *Schmidtea mediterranea*. *Science*, *360*(6391), eaaq1736. https://doi.org/10.1126/science.aaq1736

González-Estévez, C., Momose, T., Gehring, W. J., & Saló, E. (2003). Transgenic planarian lines obtained by electroporation using transposon-derived vectors and an eye-specific GFP marker. *Proceedings of the National Academy of Sciences of the United States of America*, *100*(24), 14046–14051. https://doi.org/10.1073/pnas.2335980100

Grohme, M. A., Schloissnig, S., Rozanski, A., Pippel, M., Young, G. R., Winkler, S., Brandl, H.,

Henry, I., Dahl, A., Powell, S., Hiller, M., Myers, E., & Rink, J. C. (2018). The genome of *Schmidtea mediterranea* and the evolution of core cellular mechanisms. *Nature*, *554*(7690), 56–61. https://doi.org/10.1038/nature25473

Jeacock, L., Faria, J., & Horn, D. (2018). Codon usage bias controls mRNA and protein abundance in trypanosomatids. *eLife*, *7*, e32496. https://doi.org/10.7554/eLife.32496

Kim, I. V., Duncan, E. M., Ross, E. J., Gorbovytska, V., Nowotarski, S. H., Elliott, S. A., Sánchez Alvarado, A., & Kuhn, C. D. (2019). Planarians recruit piRNAs for mRNA turnover in adult stem cells. *Genes & Development*, *33*(21–22), 1575–1590. https://doi.org/10.1101/gad.322776.118

Lakshmanan, V., Bansai, D., Kulkarni, J., Poduval, D., Krishna, S., Sasidharan, V., Anand, P., Seshasayee, A., & Palakodeti, D. (2016). Genome-wide analysis of polyadenylation events in *Schmidtea mediterranea*. *G3: Genes, Genomes, Genetics*, *6*(10), 3035–3048. https://doi.org/10.1534/g3.116.031120

Lei, K., McKinney, S. A., Ross, E. J., Lee, H. C., & Sánchez Alvarado, A. (2019). Cultured pluripotent planarian stem cells retain potency and express proteins from exogenously introduced mRNAs. *bioRxiv*. https://doi.org/10.1101/573725

Leppek, K., Woo Byeon, G., Kladwang, W., Wayment-Steele, H. K., Kerr, C. H., Xu, A. F., Soon Kim, D., Topkar, V. V, Choe, C., Rothschild, D., Tiu, G. C., Wellington-Oguri, R., Fujii, K., Sharma, E., Watkins, A. M., Nicol, J. J., Romano, J., Tunguz, B., Participants, E., … Das, R. (2021). Combinatorial optimization of mRNA structure, stability, and translation for RNA-based therapeutics. *bioRxiv*. https://doi.org/10.1101/2021.03.29.437587

Li, P., Nanes Sarfati, D., Xue, Y., Yu, X., Tarashansky, A. J., Quake, S. R., & Wang, B. (2021). Single-cell analysis of *Schistosoma mansoni* identifies a conserved genetic program controlling germline stem cell fate. *Nature Communications*, *12*, 485. https://doi.org/10.1038/s41467-020-20794-w

Li, Y., Teague, B., Zhang, Y., Su, Z., Porter, E., Dobosh, B., Wagner, T., Irvine, D. J., & Weiss, R. (2019). *In vitro* evolution of enhanced RNA replicons for immunotherapy. *Scientific Reports*, *9*, 6932. https://doi.org/10.1038/s41598-019-43422-0

Merritt, C., Rasoloson, D., Ko, D., & Seydoux, G. (2008). 3’ UTRs are the primary regulators of gene expression in the *C. elegans* germline. *Current Biology*, *18*(19), 1476–1482. https://doi.org/10.1016/j.cub.2008.08.013

Mihaylova, Y., Abnave, P., Kao, D., Hughes, S., Lai, A., Jaber-Hijazi, F., Kosaka, N., & Aboobaker, A. A. (2018). Conservation of epigenetic regulation by the MLL3/4 tumour suppressor in planarian pluripotent stem cells. *Nature Communications*, *9*, 3633. https://doi.org/10.1038/s41467-018-06092-6

Molinaro, A. M., & Pearson, B. J. (2016). In silico lineage tracing through single cell transcriptomics identifies a neural stem cell population in planarians. *Genome Biology*, *17*(1), 87. https://doi.org/10.1186/s13059-016-0937-9

Newmark, P. A., & Sánchez Alvarado, A. (2002). Not your father's planarian: A classic model enters the era of functional genomics. *Nature Reviews Genetics*, *3*(3), 210–219. https://doi.org/10.1038/nrg759

Pascual-Carreras, E., Marín-Barba, M., Castillo-Lara, S., Coronel-Córdoba, P., Magri, M. S., Wheeler, G. N., Abril, J. F., Gomez-Skarmeta, J. L., Saló, E., & Adell, T. (2020). Genomic analyses reveal FoxG as an upstream regulator of wnt1 required for posterior identity specification in planarians. *bioRxiv*,. https://doi.org/10.1101/2020.12.08.416008

Patro, R., Duggal, G., Love, M. I., Irizarry, R. A., & Kingsford, C. (2017). Salmon provides fast and bias-aware quantification of transcript expression. *Nature Methods*, *14*(4), 417–419. https://doi.org/10.1038/nmeth.4197

Petersen, C. P., & Reddien, P. W. (2009). A wound-induced Wnt expression program controls planarian regeneration polarity. *Proceedings of the National Academy of Sciences of the United States of America*, *106*(40), 17061–17066. https://doi.org/10.1073/pnas.0906823106

Plass, M., Solana, J., Alexander Wolf, F., Ayoub, S., Misios, A., Glažar, P., Obermayer, B., Theis, F. J., Kocks, C., & Rajewsky, N. (2018). Cell type atlas and lineage tree of a whole complex animal by single-cell transcriptomics. *Science*, *360*(6391), eaaq1723. https://doi.org/10.1126/science.aaq1723

Puigbò, P., Bravo, I. G., & Garcia-Vallvé, S. (2008). E-CAI: A novel server to estimate an expected value of Codon Adaptation Index (eCAI). *BMC Bioinformatics*, *9*(1), 65. https://doi.org/10.1186/1471-2105-9-65

Quax, T. E. F., Claassens, N. J., Söll, D., & van der Oost, J. (2015). Codon bias as a means to fine-tune gene expression. *Molecular Cell*, *59*(2), 149–161. https://doi.org/10.1016/j.molcel.2015.05.035

Reddien, P. W. (2018). The cellular and molecular basis for planarian regeneration. *Cell*, *175*(2),

327–345. https://doi.org/10.1016/j.cell.2018.09.021

Reddien, P. W., Bermange, A. L., Murfitt, K. J., Jennings, J. R., & Sánchez Alvarado, A. (2005). Identification of genes needed for regeneration, stem cell function, and tissue homeostasis by systematic gene perturbation in planaria. *Developmental Cell*, *8*(5), 635–649. https://doi: 10.1016/j.devcel.2005.02.014

Rink, J. C. (2018). Stem cells, patterning and regeneration in planarians: Self-organization at the organismal scale. *Methods in Molecular Biology*, *1774*, 57–172. https://doi.org/10.1007/978-1-4939-7802-1_2

Rossi, A., Ross, E. J., Jack, A., & Sánchez Alvarado, A. (2014). Molecular cloning and characterization of SL3: A stem cell-specific SL RNA from the planarian Schmidtea mediterranea. *Gene*, *533*(1), 156–167. https://doi.org/10.1016/j.gene.2013.09.101

Rozanski, A., Moon, H. K., Brandl, H., Martín-Durán, J. M., Grohme, M. A., Hüttner, K., Bartscherer, K., Henry, I., & Rink, J. C. (2019). PlanMine 3.0 - improvements to a mineable resource of flatworm biology and biodiversity. *Nucleic Acids Research*, *47*(D1), D812–D820. https://doi.org/10.1093/nar/gky1070

Sánchez Alvarado, A., & Newmark, P. A. (1999). Double-stranded RNA specifically disrupts gene expression during planarian regeneration. *Proceedings of the National Academy of Sciences of the United States of America*, *96*(9), 5049–5054. https://doi.org/10.1073/pnas.96.9.5049

Schmiderer, L., Subramaniam, A., Žemaitis, K., Bäckström, A., Yudovich, D., Soboleva, S., Galeev, R., Prinz, C. N., Larsson, J., & Hjort, M. (2020). Efficient and nontoxic biomolecule delivery to primary human hematopoietic stem cells using nanostraws. *Proceedings of the National Academy of Sciences of the United States of America*, *117*(35), 21267–21273. https://doi.org/10.1073/pnas.2001367117

Stückemann, T., Cleland, J. P., Werner, S., Thi-Kim Vu, H., Bayersdorf, R., Liu, S. Y., Friedrich, B., Jülicher, F., & Rink, J. C. (2017). Antagonistic self-organizing patterning systems control maintenance and regeneration of the anteroposterior axis in planarians. *Developmental Cell*, *40*(3), 248–263. https://doi.org/10.1016/j.devcel.2016.12.024

Svitkin, Y. V., Cheng, Y. M., Chakraborty, T., Presnyak, V., John, M., & Sonenberg, N. (2017). N1-methyl-pseudouridine in mRNA enhances translation through eIF2α-dependent and independent mechanisms by increasing ribosome density. *Nucleic Acids Research*, *45*(10),

6023–6036. https://doi.org/10.1093/nar/gkx135

Taning, C. N. T., Christiaens, O., Li, X., Swevers, L., Casteels, H., Maes, M., & Smagghe, G. (2018). Engineered flock house virus for targeted gene suppression through RNAi in fruit flies (*Drosophila melanogaster*) *in vitro* and *in vivo*. *Frontiers in Physiology*, *9*, 805. https://doi.org/10.3389/fphys.2018.00805

Tarashansky, A. J., Xue, Y., Li, P., Quake, S. R., & Wang, B. (2019). Self-assembling manifolds in single-cell RNA sequencing data. *eLife*, *8*, e48994. https://doi.org/10.7554/eLife.48994

Tay, A., & Melosh, N. (2019). Transfection with nanostructure electro-injection is minimally perturbative. *Advanced Therapeutics*, *2*(12), 1900133. https://doi.org/10.1002/adtp.201900133

Thi-Kim Vu, J., Rink, J. C., McKinney, S. A., McClain, M., Lakshmanaperumal, N., Alexander, R., & Sánchez Alvarado, A. (2015). Stem cells and fluid flow drive cyst formation in an invertebrate excretory organ. *eLife*, *4*, e07405. https://doi.org/10.7554/eLife.07405

Vila-Farré, M., & Rink, J. C. (2018). The ecology of freshwater planarians. *Methods in Molecular Biology*, *1774*, 173–205. https://doi.org/10.1007/978-1-4939-7802-1_3

Wagner, D. E., Wang, I. E., & Reddien, P. W. (2011). Clonogenic neoblasts are pluripotent adult stem cells that underlie planarian regeneration. *Science*, *332*(6031), 811–816. https://doi.org/10.1126/science.1203983

Wang, Y., Zayas, R. M., Guo, T., & Newmark, P. A. (2007). *nanos* function is essential for development and regeneration of planarian germ cells. *Proceedings of the National Academy of Sciences of the United States of America*, *104*(14), 5901–5906. https://doi.org/10.1073/pnas.0609708104

Xie, X., Xu, A. M., Leal-Ortiz, S., Cao, Y., Garner, C. C., & Melosh, N. A. (2013). Nanostraw-electroporation system for highly efficient intracellular delivery and transfection. *ACS Nano*, *7*(5), 4351–4358. https://doi.org/10.1021/nn400874a

Zayas, R. M., Bold, T. D., & Newmark, P. A. (2005). Spliced-leader trans-splicing in freshwater planarians. *Molecular Biology and Evolution*, *22*(10), 2048–2054. https://doi.org/10.1093/molbev/msi200

Zeng, A., Li, H., Guo, L., Gao, X., McKinney, S., Wang, Y., Yu, Z., Park, J., Semerad, C., Ross, E., Cheng, L. C., Davies, E., Lei, K., Wang, W., Perera, A., Hall, K., Peak, A., Box, A., & Sánchez Alvarado, A. (2018). Prospectively isolated tetraspanin$^{+}$ neoblasts are adult

pluripotent stem cells underlying planaria regeneration. *Cell*, *173*(7), 1593–1608. https://doi.org/10.1016/j.cell.2018.05.006

# Main Figures

## Figure 1

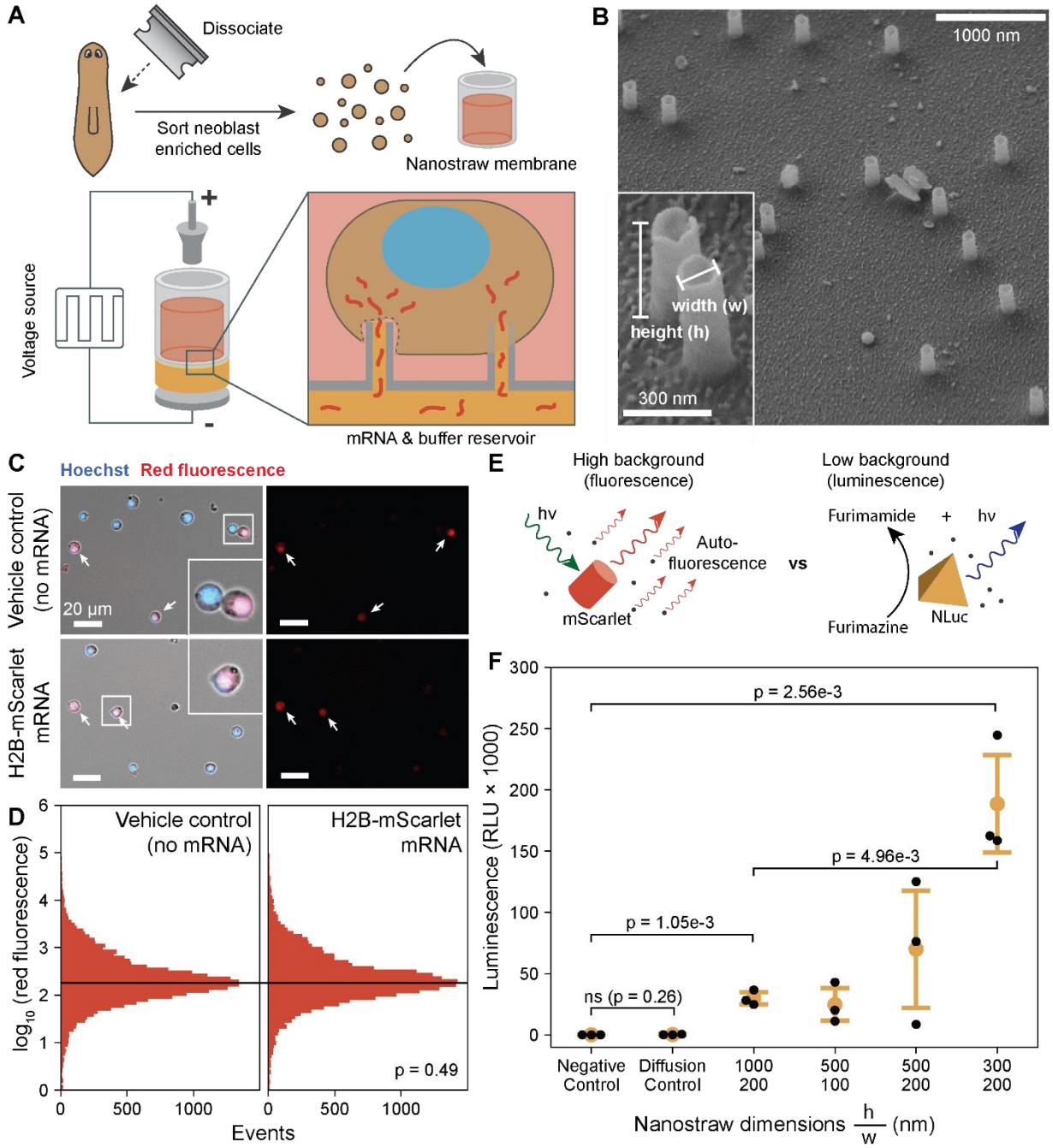

**Figure 1: Nanoluciferase mRNA delivered through nanostraws is expressed in planarian cells.** (**A**) Schematics showing the steps of nanostraw electro-delivery. In each experiment, 200,000 cells are placed into a nanostraw cartridge. (**B**) SEM images of nanostraws. Inset: a magnified view showing individual straws. (**C**) Epi-fluorescence images showing planarian cells after nanostraw delivery. Insets: magnified views showing cells with nuclear autofluorescence. Arrows: example red autofluorescent cells. (**D**) Histogram of red fluorescence measured by flow cytometry. Both samples show nearly identical distributions. Statistical insignificance ($p = 0.49$, t-test) was established by bootstrapping, which calculates the p-value for 10,000 random subsamples of 100 cells between both distributions. (**E**) Unlike autofluorescence, autoluminescence is absent in planarian tissues, making luminescent reporters easy to detect. (**F**) Luminescence measured from 200,000 cells on a plate reader at 24 hr post nanostraw delivery with sNluc1 mRNA via the addition of furimazine, the substrate utilized by Nluc. Cells were subjected to 45 s of a square wave pulse train of 35 V, 200 μs, and 40 Hz applied 3 times with 1 min between each cycle to inject the cargo. Each data point represents one biological replicate which was conducted on an independently isolated population of cells using nanostraws from the same batch and mRNA synthesized in the same reaction. Negative control: nanostraw delivery with PBS alone. Diffusion: mock experiments without applying electrical pulses. Error bars represent the standard deviation and p-values were calculated using two-sided Welch's t-test.

**Figure 2**

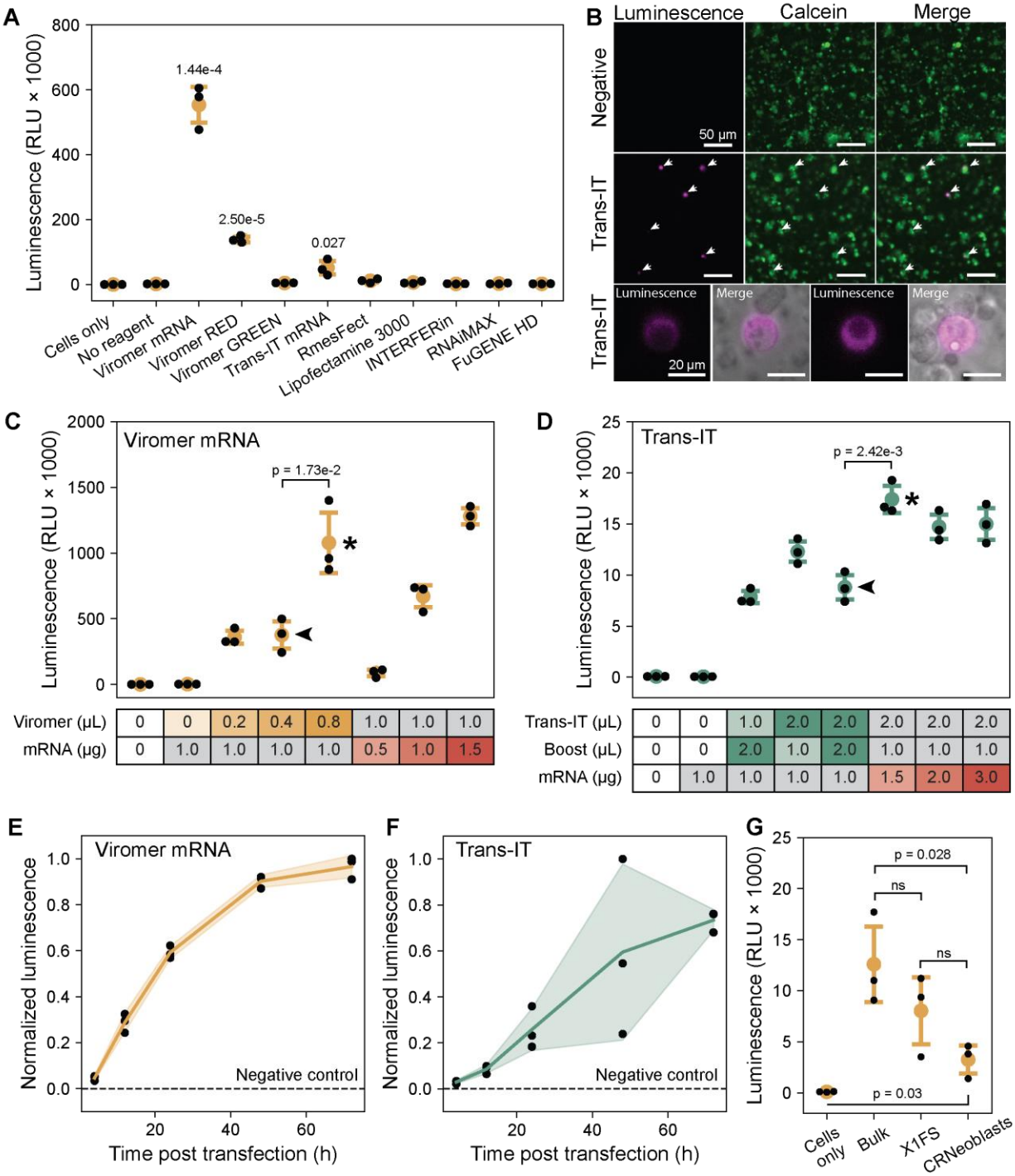
A
Luminescence (RLU × 1000)
800
600
400
200
0
1.44e-4
2.50e-5
0.027
Cells only
No reagent
Viromer mRNA
Viromer RED
Viromer GREEN
Trans-IT mRNA
RmesFect
Lipofectamine 3000
INTERFERin
RNAiMAX
FuGENE HD
B
Luminescence
Calcein
Merge
Negative
Trans-IT
Trans-IT
50 µm
Luminescence
Merge
Luminescence
Merge
20 µm
C
Viromer mRNA
Luminescence (RLU × 1000)
2000
1500
1000
500
0
p = 1.73e-2
*
Viromer (µL) 0 0 0.2 0.4 0.8 1.0 1.0 1.0
mRNA (µg) 0 1.0 1.0 1.0 1.0 0.5 1.0 1.5
D
Trans-IT
Luminescence (RLU × 1000)
25
20
15
10
5
0
p = 2.42e-3
*
Trans-IT (µL) 0 0 1.0 2.0 2.0 2.0 2.0 2.0
Boost (µL) 0 0 2.0 1.0 2.0 1.0 1.0 1.0
mRNA (µg) 0 1.0 1.0 1.0 1.0 1.5 2.0 3.0
E
Viromer mRNA
Normalized luminescence
1.0
0.8
0.6
0.4
0.2
0.0
Negative control
20
40
60
Time post transfection (h)
F
Trans-IT
Normalized luminescence
1.0
0.8
0.6
0.4
0.2
0.0
Negative control
20
40
60
Time post transfection (h)
G
Luminescence (RLU × 1000)
25
20
15
10
5
0
p = 0.028
ns
ns
p = 0.03
Cells only
Bulk
X1FS
CRNeoblasts

**Figure 2: A screen identified chemical reagents to efficiently transfect planarian cells.** (**A**) Luminescence from 200,000 cells transfected with 1 µg of YB1-sNluc1 mRNA across a range of chemical transfection reagents, using manufacturer's recommended protocols (**Supplementary Table 2)**. p-values were calculated by comparing experimental groups with the negative control in which mRNA was delivered with no transfection reagent. (**B**) Luminescence images of planarian cells transfected with YB1-sNluc1 mRNA using Trans-IT mRNA. Cells were imaged on an Olympus LV200 luminescence microscope with either a 20× air objective (Olympus: UPLXAPO20X) for a large field of view or a 100× oil immersion objective (Olympus: UPLXAPO100XO) to observe subcellular localization. Cells were stained with 4 ng/µL Calcein AM (green) with luminescence shown in magenta. Optimization of (**C**) Viromer mRNA and (**D**) Trans-IT mRNA transfections identified conditions with increased expression that are used for all following experiments (asterisk), compared to the condition initially used in the screen (arrowheads). 200,000 cells were transfected in each experiment. (**E**) Viromer mRNA and (**F**) Trans-IT transfected cells showing gradual increase of luminescence over time. Luminescence was measured on 200,000 cells per replicate at each time point and normalized against the maximum luminescence across replicates. The dashed line marks the mean intensity of the negative controls (n = 3) using only furimazine substrate and mRNA in the absence of any transfection reagent. Shaded regions: standard deviation. (**G**) Luminescence from 40,000 sorted neoblast enriched cells or bulk sorted cells transfected with YB1-sNluc1 mRNA. In all experiments, cells were transfected with 1 µg of YB1-sNluc1 mRNA unless otherwise specified (**Supplementary Table 3**), assayed for luminescence at 24 hpt. Data point in panels **A** and **G** represents the mean luminescence of three parallel technical replicates, and the experiments were conducted on three biological replicates each using independently dissociated cells. Data points in panels **C-F** are from technical replicates. p-values were calculated using two-sided Welch's t-test.

**Figure 3**

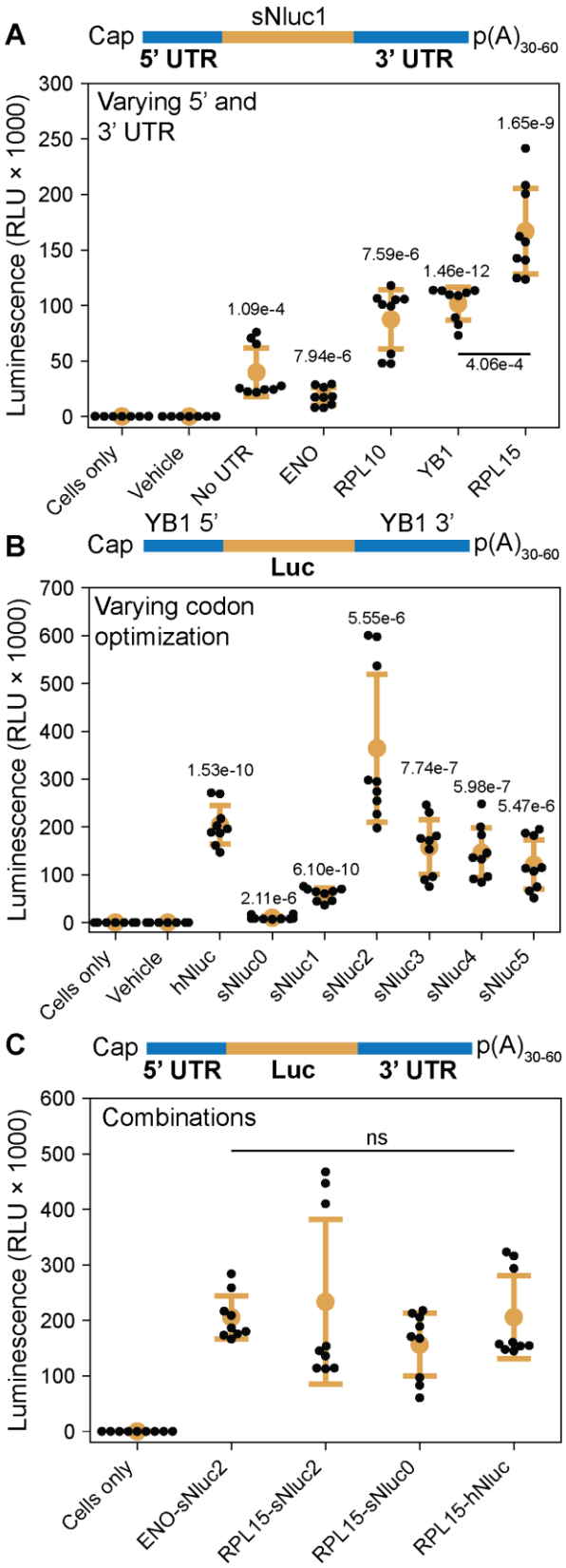
A
Cap
sNluc1
p(A)30-60
5' UTR
3' UTR
Varying 5' and 3' UTR
Luminescence (RLU × 1000)
1.09e-4
7.94e-6
7.59e-6
1.46e-12
4.06e-4
1.65e-9
Cells only
Vehicle
No UTR
ENO
RPL10
YB1
RPL15
B
Cap
YB1 5'
YB1 3'
Luc
p(A)30-60
Varying codon optimization
1.53e-10
2.11e-6
6.10e-10
5.55e-6
7.74e-7
5.98e-7
5.47e-6
hNluc
sNluc0
sNluc1
sNluc2
sNluc3
sNluc4
sNluc5
C
Cap
5' UTR
Luc
3' UTR
p(A)30-60
Combinations
ns
ENO-sNluc2
RPL15-sNluc2
RPL15-sNluc0
RPL15-hNluc

**Figure 3: Expression of exogenously delivered mRNA is regulated post-transcriptionally.** (**A**) Luminescence from transfections using a range of constructs incorporating different endogenous 5' and 3' UTRs flanking sNluc1. No-UTR mRNA contains flanking attB1 and attP1 sequences used for cloning. UTRs were cloned from ENO, enolase (dd_Smed_v6_510_0_1); RPL10, ribosomal protein L10 (dd_Smed_v6_130_0_1); YB1, YB1 cold shock protein (dd_Smed_v6_52_0_1); RPL15, ribosomal protein L15 (dd_Smed_v6_193_0_1), which were identified using the gene annotation provided by PlanMine (Rozanski et al., 2019). (**B**) Luminescence from alternative codon usage variants of Nluc flanked by YB1 UTR. (**C**) Luminescence from transfections using constructs that combine various UTRs with Nluc codon variants. Note the expression showed no significant differences. All transfections were performed across three biological replicates consisting of three technical replicates with 200,000 cells, from whole dissociated planarians, using 1 µg mRNA and 0.8 µL Viromer per well. Each biological replicate was performed with mRNA produced from independent *in vitro* synthesis reactions. Luminescence was assayed 24 hpt. (In **A** and **B**, p-values were calculated using two-sided Welch's t-test between experimental groups and negative controls with cells only; in **C** statistical insignificance was established using Tukey's HSD pairwise t-test.

**Figure 4**

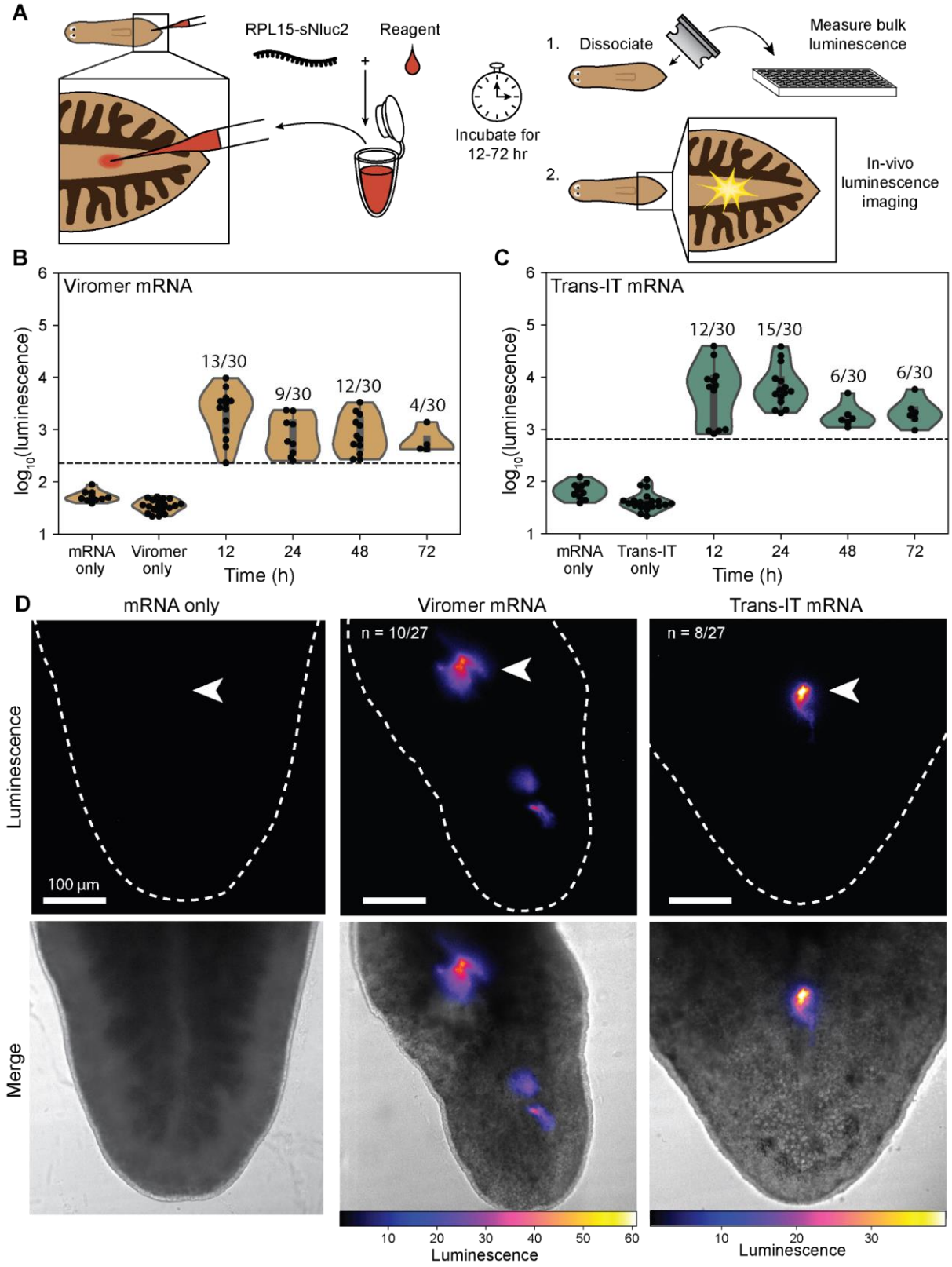
A
RPL15-sNluc2
Reagent
Incubate for 12-72 hr
1. Dissociate
Measure bulk luminescence
2.
In-vivo luminescence imaging
B
Viromer mRNA
log10(luminescence)
13/30
9/30
12/30
4/30
mRNA only
Viromer only
12
24
48
72
Time (h)
C
Trans-IT mRNA
12/30
15/30
6/30
6/30
mRNA only
Trans-IT only
Time (h)
D
mRNA only
Viromer mRNA
Trans-IT mRNA
n = 10/27
n = 8/27
Luminescence
Merge
100 µm
Luminescence

**Figure 4: Heterologous reporter expression *in vivo*.** (**A**) Schematics showing the workflow of *in vivo* transfection experiments. Bulk luminescence was measured from dissociated worms injected with mRNA complexed with (**B**) Viromer mRNA or (**C**) Trans-IT mRNA. Dashed lines: 3 standard deviations above the background (based on the mRNA only condition) to discriminate negative and positive animals. Numbers of positive animals out of all animals injected are reported for each time point. Viromer was prepared with 0.8 µL of Viromer, 1 µg of RPL15-sNluc2 mRNA, and Viromer Buffer up to a final reaction volume of 25 µL. Trans-IT was prepared with 2 µL of Trans-IT, 1 µL of Boost, 1.5 µg of RPL15-sNluc2 mRNA, in L-15 up to a final volume of 25 µL. 30 worms, from two independent experiments, were injected along the tail midline with 0.9 µL of transfection mix per time point per transfection reagent. (**D**) Live planarians imaged on the Olympus LV200 luminescence microscope through a 20× air objective (NA 0.8, WD 0.6 mm, Olympus: UPLXAPO20X). 27 worms were injected per transfection reagent while negative control worms were injected with mRNA alone. Images were acquired at 12 hpt. Worms were anesthetized and incubated for 15 min in furimazine (NanoGlo-Live, Promega) supplemented with 1% DMSO to aid in permeabilization. Luminescence images were acquired using an exposure of 1 min. Brightfield images were acquired using an exposure of 10 ms. All experiments were performed using identical exposure time and digital gain. Dashed lines: worm tail boundary; arrows: the site of the injection. n: number of injections that produced visible, localized luminescence signal out of total injected animals.

## Supplementary figures

**Figure 1 – figure supplement 1: Nanostraw electro-delivery device.**

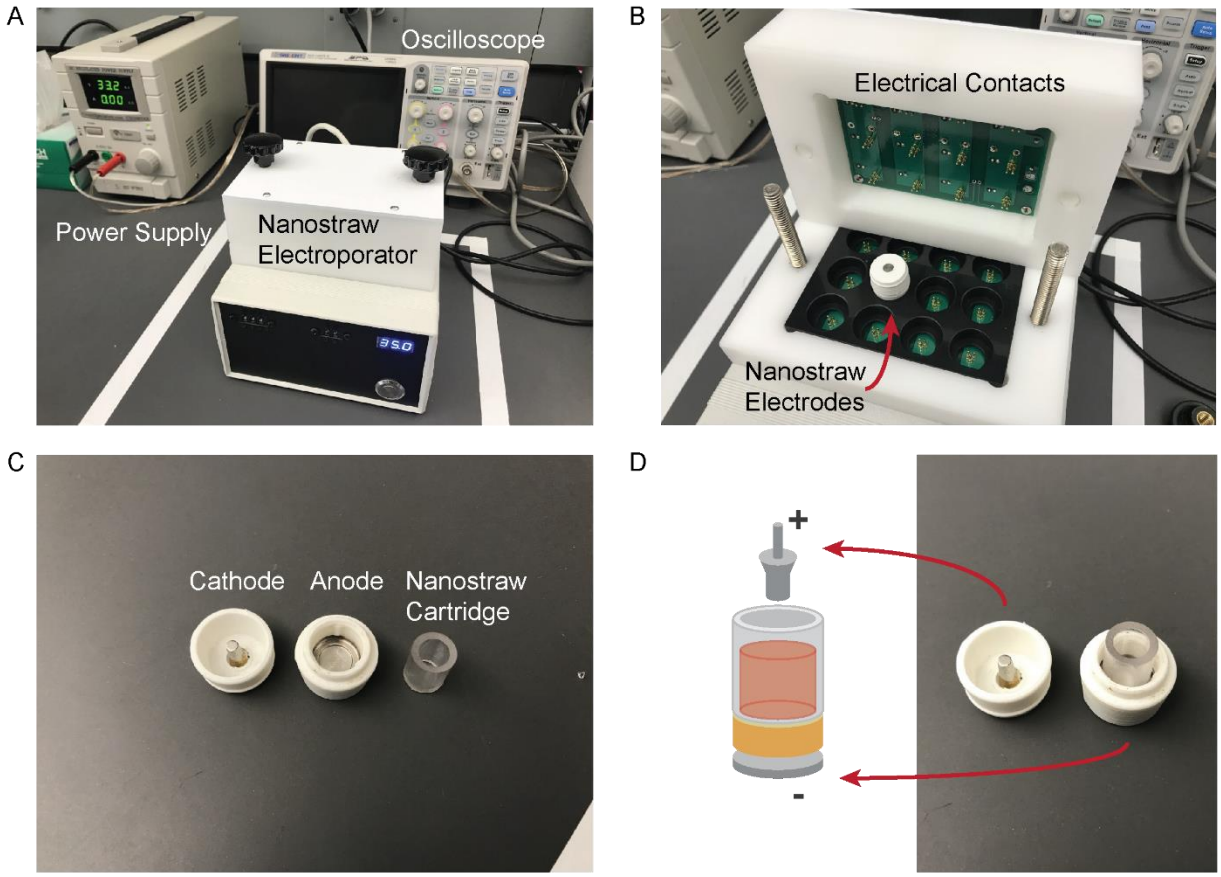


**Figure 1 – figure supplement 1: Nanostraw electro-delivery device.** (A) A photograph of the nanostraw device. In frame is the power supply (left), the oscilloscope, which is used to monitor the square wave pulses (top right), and the nanostraw electroporator device (center bottom) showing the dials to set the pulse width, duration, and voltage. (B) An interior view of the nanostraw device, showing the electrical contacts which interface with the nanostraw electro-delivery cartridge and carry the electrical pulses to the titanium electrodes on the top and bottom of the cartridge. (C) Individual components of the nanostraw cartridge, showing the cathode, which dips into the cell culture medium from above, the anode, which sits just below the buffer and mRNA to be delivered, and the nanostraw membrane, which is inserted atop the buffer and anode. (D) A demonstration of a nanostraw membrane placed within the cartridge.

**Figure 2 – Figure supplement 1: CRNeoblast sorting and validation.**

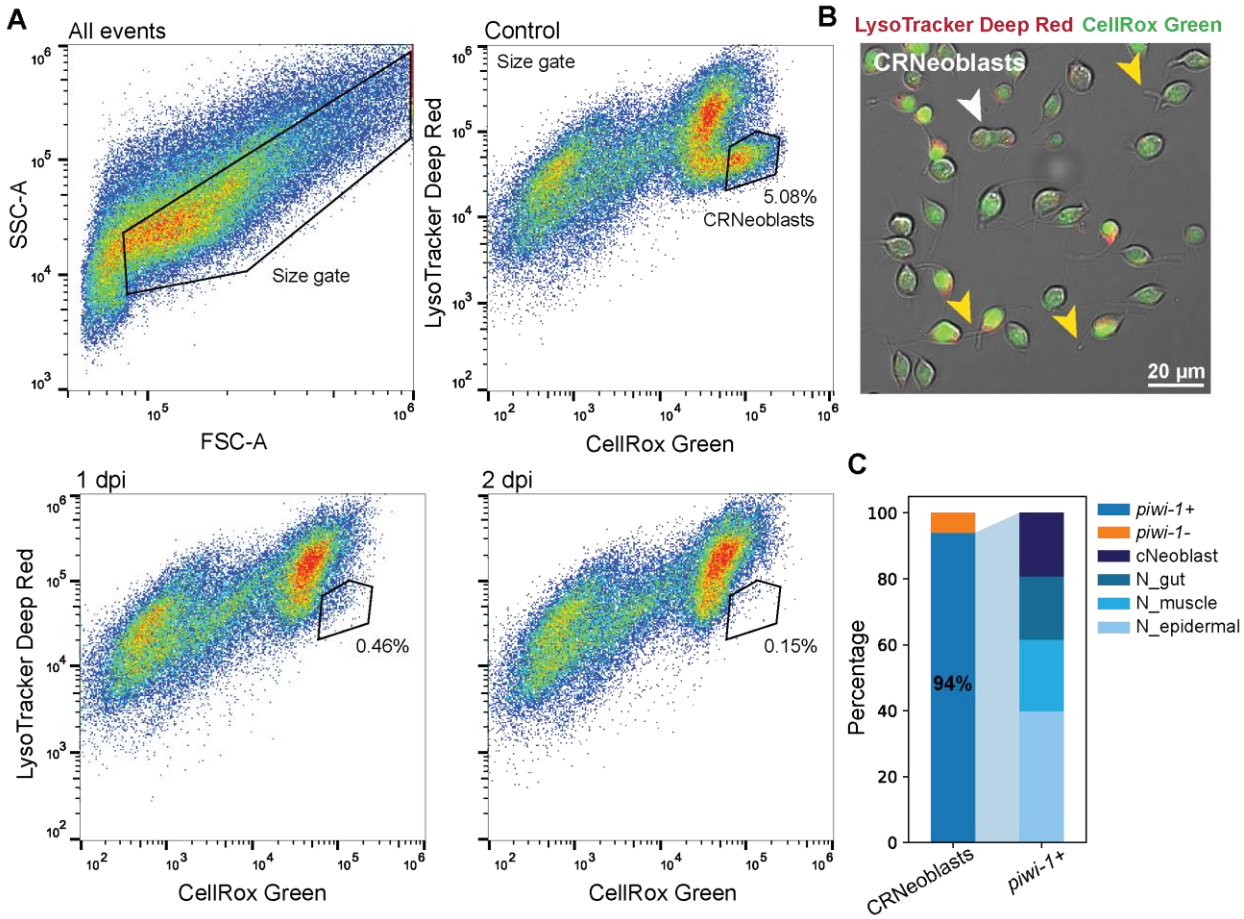


**Figure 2 – figure supplement 1: CRNeoblast sorting and validation.** (A) FACS gates to sort for CRNeoblasts and their susceptibility to irradiation. The cells are first gated by forward and side-scatter (FSC-A, SSC-A) to remove larger somatic cells. Small cells are then gated for high CellRox Green (it binds to DNA upon oxidation) and low LysoTracker Deep Red (it binds to intracellular membranes) fluorescence intensity. This strategy is designed to select for cells with high DNA content (i.e., cells in S or $G_2$/M phase) and low organelle complexity. Unlike other DNA binding dyes, we found that CellRox Green has a very low toxicity level. CRNeoblasts make up approximately 5% of the total events detected. Upon x-ray irradiation (20 Gy), this population significantly diminishes in size and is nearly completely ablated by two days post irradiation (dpi). (B) Sorted CRNeoblasts have uniform morphology. White arrowhead: an example CRNeoblast in the process of dividing. Yellow arrowheads: processes that are characteristic of planarian neoblasts. (C) Single cell RNA-sequencing analysis of CRNeoblasts show that ~94% were positive for the neoblast marker *piwi-1*. Of these *piwi-1*$^+$ cells, they were

split between neoblast subpopulations including epidermal, muscle, and gut progenitors (N_epidermal, N_muscle, and N_gut), and clonogenic neoblasts (cNeoblasts, *tgs*$^{+}$).

**Figure 3 – Figure supplement 1: Cloning methodology.**

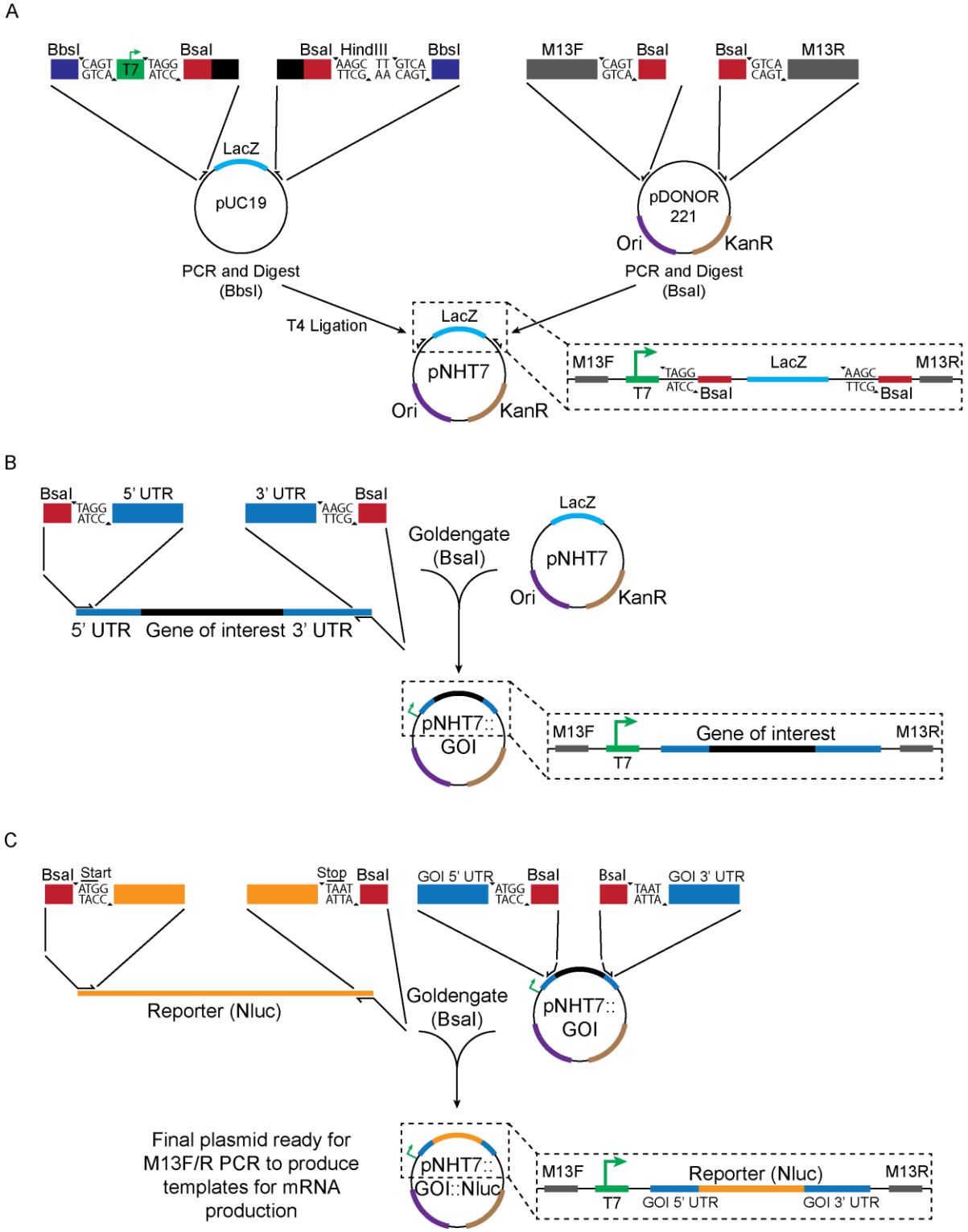

**Figure 3 – figure supplement 1: Cloning methodology.** (A) A diagram showing the steps of generating pNHT7, the base vector used to clone endogenous planarian genes. The overall design is a LacZ cassette, derived from pUC19, flanked by BsaI restriction sites, which allow for subcloning of planarian genes into pNHT7. Upstream is a T7 promoter, which allows for *in vitro* transcription (IVT), and all of these are flanked by M13 forward and reverse primers which are used to generate linearized templates for IVT through PCR. The backbone for pNHT7 is derived from the backbone from pDONOR221. (B) Isolating the 5' and 3' UTRs of a gene of interest (GOI) from cDNA uses primers containing pNHT7 compatible BsaI restriction sites followed by 5' and 3' UTR sequences of the GOI. After amplification, the fragment containing the GOI can be cloned into pNHT7 though a standard golden gate reaction. (C) The Nluc reporter is inserted between the UTR sequences by using primers containing BsaI restriction sites to prime the 5' and 3' ends of the reporter as well as outward facing primers which add complementary BsaI restriction sites and prime the end of the 5' UTR and beginning of the 3' UTR for the gene captured in pNHT7. These two amplicons can then be purified and assembled via a golden gate reaction. All primer sequences are provided in **Supplementary Table 4**.

**Figure 3 – figure supplement 2: Expected *in vitro* transcription results.**

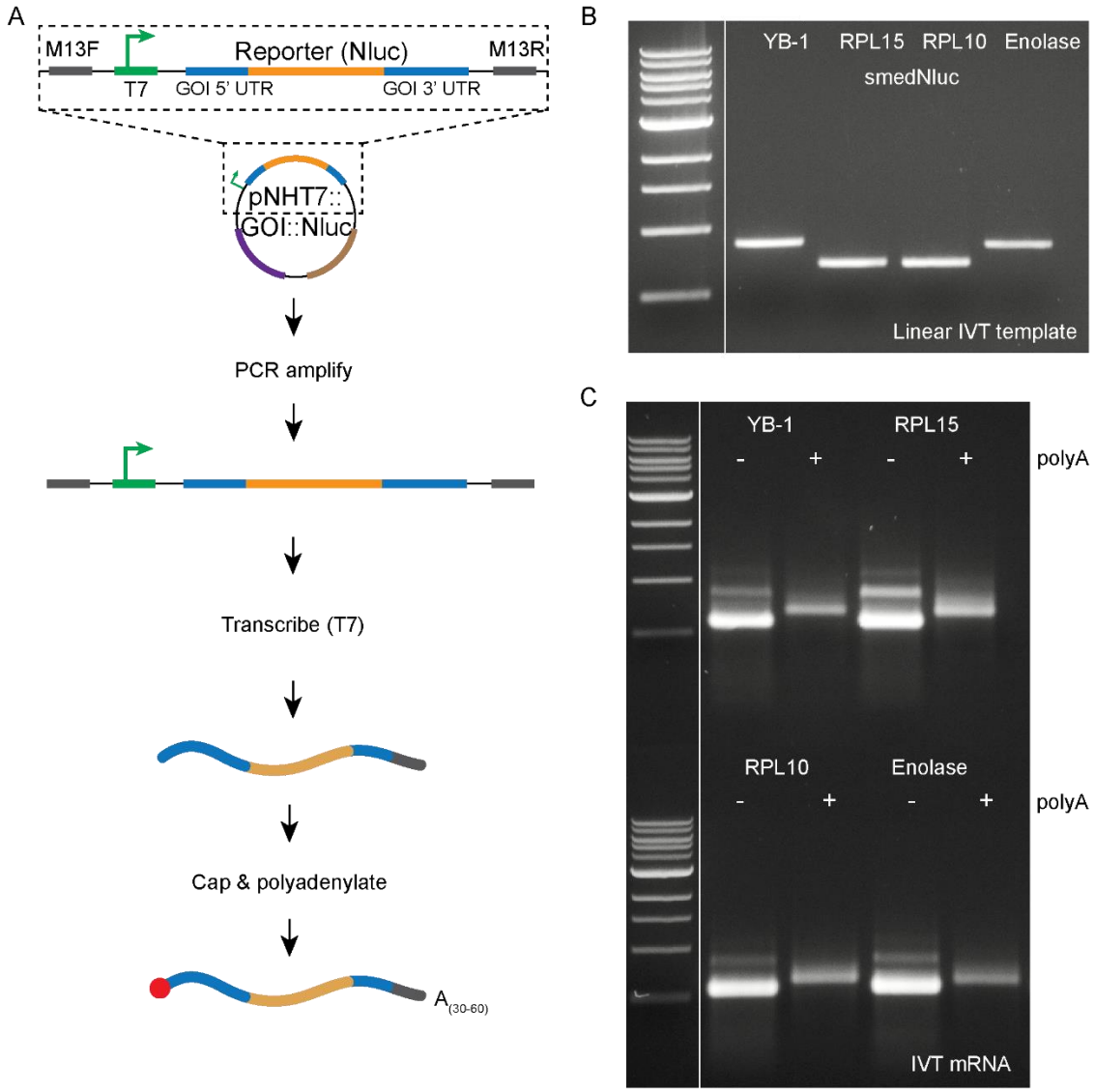


**Figure 3 – figure supplement 2: Expected *in vitro* transcription result**s. (A) Diagram of IVT. (B) EtBr stained 1% agarose gel showing the linear amplification products. (C) Gel images showing the mRNA product before and after polyadenylation. Upon successful polyadenylation, the mRNA product should be shifted in size. Samples should be free of excessive degradation products, which we found critical for successful transfections. The ladder used is the NEB 1 kb DNA ladder.

**Figure 3 – figure supplement 3: Assessment of m1Ψ on mRNA expression in planarians**

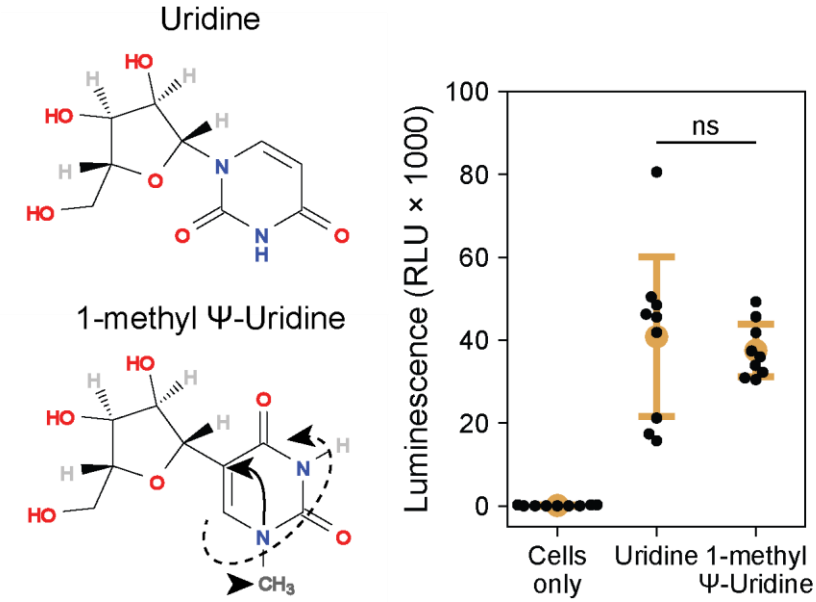


**Figure 3 – figure supplement 3: Assessment of m1Ψ on mRNA expression in planarians.** Recent reports suggest that the base analog 1-methyl pseudouridine (m1Ψ) may increase translation, improve mRNA stability, and decrease immunogenicity (Andries et al., 2015; Svitkin et al., 2017). This modification is also currently being used in recently developed mRNA vaccines against SARS-CoV-2. We compared transfections with RPL15-sNluc2 mRNA containing either rUTP or m1Ψ (chemical structures shown on the left). We found both to be active, with no significant difference between the two samples, suggesting that the observed benefits of m1Ψ modified mRNA in mammalian systems may not be directly transferrable to more basal invertebrates like planarians. Arrow: the uracil group is flipped 180 degrees and attached by a carbon-carbon bond rather than the usual carbon-nitrogen bond in pseudouridine. Arrowhead: m1Ψ contains an additional methyl group. All transfections were conducted with 0.8 µL of Viromer mRNA and 1 µg of mRNA. 200,000 cells were incubated at 20ºC, and luminescence was measured at 24 hpt. Data were collected from a single batch of cells transfected from three independent mRNA synthesis reactions across three technical replicates per batch of mRNA. We anticipate that other chemical modifications may be tested similarly in the future to identify ones which regulate gene expression in planarians.

## Supplementary table legends

**Supplementary Table 1: Nluc variants used in this study.** Coding sequences with different codon usage bias are listed with their respective GC content, and codon adaptation index (CAI) calculated from http://genomes.urv.es/CAIcal/E-CAI/.

**Supplementary Table 2: Conditions for screening transfection reagents.** The conditions followed the manufacturer's protocol. Reagent 1 is the main transfection reagent provided with the kit (e.g., Lipofectamine 3000, Trans-IT mRNA, Viromer mRNA). Reagent 2 is a reagent provided by some but not all kits. For Trans-IT this is the Boost reagent, and for Lipofectamine 3000, this is the Transfection Enhancer reagent. Diluting Buffer is the solution used to dilute the mRNA and transfection reagents. Some kits provide a specific buffer to use (Viromer) while others require serum-free medium, which is L-15 in our experiments. Incubation time was done in room temperature and is recommended to allow the reagent and mRNA to complex before adding to cells.

**Supplementary Table 3: List of constructs used in this study.** Corresponding plasmid maps are provided in GenBank (.gb) format as **Supplementary File 1**. All constructs will be made available through Addgene.

**Supplementary Table 4: Primers used in this study.** Listed are primer ID, conventional name, a short description of the usage, the sequence from 5' to 3', and the predicted melting temperature of the primer.